Materials Chemistry and Physics 162 (2015) 59–68

Contents lists available at ScienceDirect

Materials Chemistry and Physics

journal homepage: www.elsevier.com/locate/matchemphys

Deposition and characterization of graded $Cu(In_{1-x}Ga_x)Se_2$ thin films by spray pyrolysis

B.J. Babu [a, b], S. Velumani [a, c, *], A. Kassiba [b], R. Asomoza [a], J.A. Chavez-Carvayar [d], Junsin Yi [c, *]

[a] Department of Electrical Engineering-SEES, CINVESTAV-IPN, Avenida IPN 2508, San Pedro Zacatenco, D.F. C.P 07360, Mexico
[b] Institute of Molecules and Materials, UMR-CNRS 6283, Université du Maine, Avenue O. Messiaen, F-72085 Le Mans, France
[c] College of Information and Communication Engineering, Sungkyunkwan University, Suwon 440-746, Republic of Korea
[d] Instituto Investigaciones en Materiales-UNAM, Ciudad Universitario, D.F.Mexico, Mexico

HIGHLIGHTS

- Optimization of the spray deposition system for device grade chalcopyrite CIGS films.
- Optimized substrate temperature to obtain single-phase CIGS by spray deposition.
- Detailed report on compositional dependence of $CuInSe_2$ (CIS) thin films.
- Systematic analysis of the influence of Ga in CIS by spray deposition.
- Bowing parameter is extracted from the experiment values.

GRAPHICAL ABSTRACT

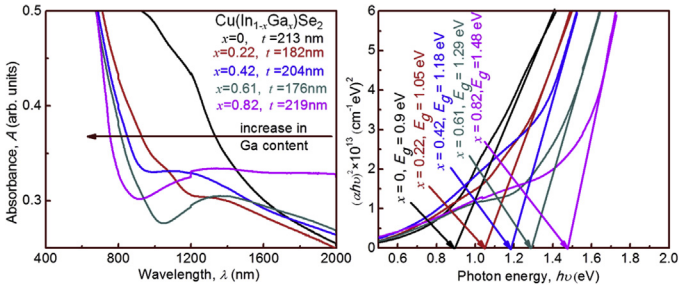

ARTICLE INFO

Article history:
Received 1 April 2014
Received in revised form
25 April 2015
Accepted 1 May 2015

Keywords:
Chemical synthesis
Coatings
Electronic materials
Thin films
Band-structure
Semiconductivity

ABSTRACT

$Cu(In_{1-x}Ga_x)Se_2$ (CIGS) thin films and their graded ($x = 1$ to 0) layer were grown on soda lime glass substrates using chemical spray pyrolysis (CSP) at different substrate temperatures (T_s). After optimization of T_s, depositions were carried out at different gallium composition (x) at optimized temperature of 350 °C. All the films deposited at $T_s \geq 350$ °C were polycrystalline chalcopyrite structure, with a preferential orientation of (112), including the graded layer. With increase in x, lattice parameters a and c were observed to decrease. Line scan of the CIGS layer showed intersection of gallium and indium concentrations, revealing the graded nature of the film. Composition dependence of Raman peak for $CuInSe_2$ (CIS) deposited by CSP was analyzed. Optical transmittance at a wavelength of 800 nm of the film with $x = 0$ (CIS) (30%) was found lower than that of the film grown with $x = 0.82$ (CIGS) (50%). Cusp-shape of the resistivity was observed with an increase of x leading to steep rise in resistivity of the films (1.61–71.68 Ω-cm) till $x = 0.42$ and then decreased to 4.78 Ω-cm at $x = 0.82$. Carrier concentrations of the films were evaluated in the order of 10^{16}–10^{19} cm^{-3} with p-type conductivity. These results indicate that graded CIGS thin films with modulated gallium composition can be prepared by CSP.

1. Introduction

Ternary chalcopyrite semiconductors of I-III-VI_2 group have attracted considerable attention over the last two decades, because

* Corresponding authors. CINVESTAV –IPN, Ave IPN 2508, Col Zacatenco, DF Mexico, CP 07360, Mexico and College of Information and Communication Engineering, Sungkyunkwan University, Suwon 440-746, Republic of Korea.
E-mail addresses: velu@cinvestav.mx, vels64@yahoo.com (S. Velumani), yi@yurim.skku.ac.kr (J. Yi).

http://dx.doi.org/10.1016/j.matchemphys.2015.05.001
0254-0584/

of their potential application in optoelectronic devices, particularly in solar cells [1–10]. Among the same family of materials, $CuInSe_2$ (CIS) and $CuGaSe_2$ (CGS) have proved to be effective and stable light absorbers for the fabrication of heterojunction solar cells [1]. The band gap of CIS (1.04 eV) is well below the optimum value (1.4 eV) suitable for efficient energy conversion. Alloying with Ga [2], S [3] or Al [4] increases the band gap of CIS making it more suitable for high-efficiency single junction and multi-junction devices [1]. Solar cells based on polycrystalline $Cu(In,Ga)Se_2$ (CIGS) absorber layers have yielded the highest conversion efficiency among all thin-film technologies [6–8,10]. Composition gradient in the absorber layer is the main reason for inferior performance and by adjusting it appropriately, very high efficiencies can be obtained [7,8]. Researchers at Stuttgart's Centre for Solar Energy and Hydrogen Research (ZSW) recently achieved 21.7% efficiency with a new CIGS solar cell [6]. Advanced co-evaporation technique gives the best control of composition and compositional grading throughout the films [11]. The highest CIGS cell efficiency was obtained by a three-stage co-evaporation process [5–10]. However, the high cost of vacuum-based fabrication process and low utilization of source material becomes a barrier to make affordable commercial modules [12].

An efficient, simple, low cost non-vacuum processes such as electrodeposition, screen printing, spin-coating, doctor blade and spray pyrolysis has the potential to overcome this barrier. Several low cost techniques have already been recording efficiencies of 11–15% in the recent years [12,13]: co-electrodeposited CIGS absorber with 13.8% (0.48 cm^2) efficiency was reported for an industrial process on flexible substrates [14], Nanosolar has reported 14% efficient CIGS cells using mixed selenide nano-particles and a single-stage annealing treatment [15]. Guo et al. [16] utilized multinary sulfide nanocrystal ink deposition followed by annealing in a selenium atmosphere to produce high performance ($\eta = 12.0\%$) thin film $Cu(In_{1-x}Ga_x)$ (S_ySe_{2-y}) based photovoltaic devices, the power conversion efficiency of 15.2% (the highest published value for a pure solution deposition technique for any photovoltaic absorber material) was reported for a hydrazine-processed CIGS solar cell [13] and the record for efficiency remains with the 5% energy conversion efficiency reported by Duchemin et al. [17] for a CIS device deposited using spray pyrolysis. Improved control of the Ga profile in the CIGS layers might lead to improved device efficiencies. This is likely to be difficult for particulate and electrodeposition techniques, though the hydrazine technique has already been used to demonstrate CIGS layers with controlled Ga depth profile [12]. However hydrazine is highly reactive and toxic material, the precursor preparation and deposition must be achieved under an inert atmosphere.

CIGS layer deposition is the most challenging step for low cost cell processing, since it is the most critical layer of the cell. Selection of metal salts (e.g. chlorides and nitrates) offers the easy and the most intuitive ways to introduce the various constituent elements into a CIGS precursor solution, since these salts offer good solubility in water and alcohol. In the absence of binding agent, this type of solution has low viscosity and therefore spray pyrolysis (pneumatic, ultrasonic or electrostatic) is typically used to produce a thick film [12]. Spray pyrolysis of CIGS is based on the decomposition and reaction of premixed precursors, generally metal-chlorides and a chalcogen compound (typically n, n-dimethyl selenourea or selenourea), on a heated substrate (300–400 °C) [11,12]. Earlier attempts to prepare the solid solutions of I-III-VI_2 compounds by spray pyrolysis were made by Pamplin and Feigelson [18] and Tiwari et al. [19] and they succeeded in depositing sphalerite forms of $CuGaS_2$, $CuInS_2$, CIS and CGS. This was followed by a considerable number of investigations that were carried out for the preparation and characterization of CIS films deposited by spray pyrolysis [17–24]. The use of $CuCl_2$ in place of CuCl was reported to lead enhanced formation of chalcopyrite phase $CuInSe_2$ [20]. Substrate temperature (T_s) is a very crucial parameter during the deposition of CIGS using spray pyrolysis. At temperatures below 300 °C, impurities from the precursor (i.e. C, Cl, N) remain in the resulting films at unacceptably high levels. Above approximately 400 °C, a loss of S and Se has typically been noted, resulting in the formation of oxides [12,18].

Although spray pyrolysis technique is one of the best investigated non-vacuum deposition processes (mainly for CIS), only few reports are available for CIGS thin films [25–28]. Prior to this work, CIGS nanopowders and thin films were fabricated by our group, using non-vacuum processes such as mechano-chemical alloying [29–31], screen-printing [30] and spray pyrolysis [32,33]. In the present work, we report optimization of T_s to obtain single phase CIGS thin films on glass substrate using spray pyrolysis technique. Structural, optical and electrical properties of CIGS thin films with different gallium alloy composition (x) and Cu stoichiometry were also discussed. The optical band gap of CIGS thin films increased with an increase in gallium content (x), revealing homogeneous incorporation of gallium into chalcopyrite lattice. Also, for first time, we report deposition of graded CIGS layer by chemical spray pyrolysis (CSP) and its systematic characterizations.

2. Experimental procedure

CIGS thin films were prepared by CSP, using 20 vol. % aqueous ethanol (Fermont) solution containing copper chloride ($CuCl_2 \cdot 2H_2O$), indium tri chloride ($InCl_3$), gallium tri chloride ($GaCl_3$) and n, n dimethyl selenourea ($C_3H_8N_2Se$) as the precursor solutions. All compounds are analytical grade from Sigma Aldrich, USA and used without further purification. Concentrations of $CuCl_2$ and $GaCl_3/InCl_3$ were maintained at 0.0015 M, while that of selenourea was 0.0055 M. The [Cu]:([Ga] + [In]):[Se] atomic ratio in the solution was maintained at 1:1:3.5. An excess of n, n dimethyl selenourea was added to the precursor, in order to compensate the loss of selenium, due to its high vapor pressure. A detailed chemical reaction involved in the formation of CIS compound during spray pyrolysis using above chemicals is given by Brown et al. [24]. Similarly CIGS compound formation can be formularized as follows:

$$\begin{aligned} &CuCl_2(aq) + (1-x)InCl_3(aq) + x\,GaCl_3(aq) \\ &\quad + 3\,NH_2(CH_3)_2NCSe(aq) + 6H_2O \\ &= Cu(In_{1-x}Ga_x)Se_2(s) + 3(CH_3)_2NH(g) + 3NH_3(g) + 3CO_2(g) \\ &\quad + H_2Se(g) + 4HCl(g) + 1/2Cl_2(g) \end{aligned} \tag{1}$$

In order to study the effect of T_s and to determine optimum T_s, depositions were carried out with $x = 0.5$, at temperatures ranging from 250 to 400 °C. All the depositions were carried out for 25 min, keeping the source to substrate distance at 25 cm. CIGS thin films with $x = 0$ (CIS) to 1 (CGS) and graded CIGS layer (5 layers × 25 min) were deposited onto glass substrate at 350 °C. The solution was sprayed at a flow rate of 6.5 ml/min and nitrogen was used as the carrier gas, at a pressure of 0.11 MPa. The entire deposition process was carried out in dark inside a deposition chamber to avoid the dissociation of selenourea into elemental selenium.

Structural characterization of deposited CIGS films was carried out, using PANalytical Xpert X-Ray Diffractometer, with $CuK_{\alpha 1}$ ($\lambda = 1.5406$ Å) and $CuK_{\alpha 2}$ ($\lambda = 1.5444$ Å) lines in θ–2θ mode. X-ray diffraction (XRD) patterns were recorded in the scanning range of 20–80° with a scan step size of 0.04923°. Crystallite sizes (D) are roughly calculated using the Scherrer's formula,

$$D = 0.94\lambda/\beta \cos\theta, \quad (2)$$

where β, is full width at half maximum (FWHM) intensity of reflected peak at the Bragg angle, θ. Strain (ε) is also evaluated using the relation

$$\beta = [\lambda/(D \cos\theta)] - \varepsilon \tan\theta, \quad (3)$$

and the dislocation density (δ) is defined as the length of dislocation lines per unit volume of the crystal and can be evaluated from Equation (4)

$$\delta = 1/D^2. \quad (4)$$

The Surface morphology of the films was examined by Carl Zeiss AURIGA Field emission scanning electron microscopy (FESEM) workstation, with an operating voltage of 5 kV. Cross-sectional FESEM images were taken and allow measurements of the film thickness. The composition of all the deposited films were determined using Bruker energy dispersive analysis of X-ray (EDAX) system, attached to a secondary electron microscope, with an accelerating voltage of 20 kV. Raman studies were performed using Horiba-Jobin Yvon equipment, model LabRAM HR800 with He–Ne laser operated at 632 nm of 20 mW, but limited to 5 mW at the sample. Optical absorption spectra of CIGS thin films have been recorded as a function of wavelength, in the range between 400 and 2000 nm, by Cary 5G UV–Vis–NIR spectrophotometer. Hall measurements were carried out by the Van der Pauw method, using a Walker scientific HV-4H equipment, at room temperature. I–V measurements were performed, using Keithley 6487 picoammeter/voltage source and Lakeshore 330 auto tuning temperature controller.

3. Results and discussion

3.1. Optimization of substrate temperature (T_s)

CIGS with sphalerite or chalcopyrite phase can be obtained without any secondary phases such as Cu_2Se, $Cu_{2-x}Se$ or In_2Se_3 depending upon the deposition conditions like, the substrate temperature (T_s), acidity (pH), ionic ratio (R) and Cu precursors in the starting solutions. The effects of T_s, pH and R on CIS and CIGS thin films using CSP were investigated by several authors [18,19,21,25,27,34]. Based on their investigations we have synthesized CIGS thin films at different T_s ranging from 250 to 400 °C and determined the optimum value of 350 °C to obtain single phase CIGS thin film on the basis of following characterizations.

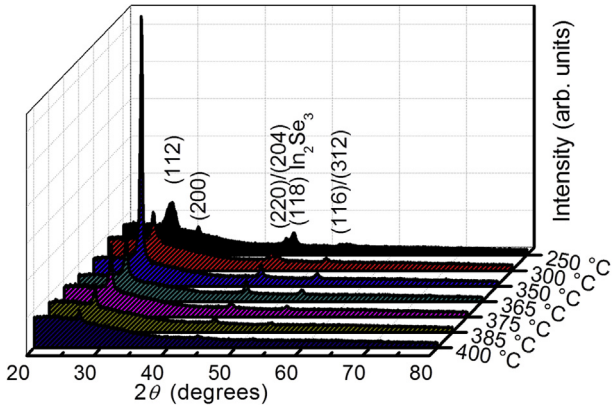

Fig. 1. XRD patterns of CIGS thin film with gallium (x) = 0.5 in the precursor solution deposited at different substrate temperatures (T_s).

Fig. 1 presents the XRD patterns of CIGS thin films deposited at different T_s, ranging from 250 to 400 °C. As T_s increases there is an improvement in the crystallinity of the films with the elimination of secondary phase such as InSe, consequently leading to the strong preferential orientation along the (112) direction [18]. At 250 and 300 °C secondary phase of InSe, was formed along with CIGS, which was depicted in the diffraction patterns shown in Fig. 1, which matched well with joint committee on powder diffraction standards data card number 23-0294 and 40-1488 (x = 0.5), respectively. Other diffraction lines of InSe phase hindered due to overlapping of CIGS peaks. Pure CIGS single phase was formed above 350 °C with lattice planes assigned to (112), (220)/(204) and (116)/(312). As temperature increases, amorphous phase was observed due to signals arising from glass substrate at lower diffraction angle. It was also observed that there is decrease in thickness of the CIGS film due to re evaporation of selenium because of its higher vapor pressure [19]. Growth rate decreased from 19.44 nm/min to 2 nm/min, when the T_s is increased from 350 to 400 °C. From the observations made by Pamplin et al. [18] and our XRD results, we noticed that films deposited by spray pyrolysis above 350 °C are not well crystalline and do not adhere well on the substrate due to re-evaporation of selenium at higher temperatures. Thus based on the above discussion we confirm that the T_s of 350 °C will be optimum, since at $T_s \leq 300$ °C thin films were formed with secondary phases; whereas above 350 °C growth rate was very slow, with poor crystallinity.

According to Table 1, 2θ values shifted towards lower angles with an increase in FWHM, due to increased strain induced by higher temperature. Crystallite size decreased and dislocation density increased with increase in T_s, indicating poor crystallinity of the films [18]. Fig. 2 shows the optical absorption curves, for samples prepared at different temperatures. An absorption edge at a value of 1.23 eV (1008 nm) for CIGS thin film deposited at 350 °C and similar edges were observed for samples deposited in the temperature range of 350–385 °C. Due to structural disorder, quite flat background was noticed for 400 °C specimen. Similar observations were made by Pamplin et al. [18] for CIS films deposited by spray pyrolysis at T_s of 200 and 400 °C. The absorption coefficient was calculated using the transmittance (T) value measured for a particular wavelength, and the film thickness (t), using the relation,

$$\alpha = -\ln(T)/t \quad (5)$$

From the plot of $(\alpha h\nu)^2$ versus $(h\nu)$ (inset of Fig. 2) the band gaps of CIGS thin films deposited at 350, 365, 375, 385 and 400 °C were found to be 1.23, 1.11, 0.97, 0.95 and 0.82 eV, respectively. The low band gap value for the films deposited at high temperature appears to be linked to structural imperfections. Indeed, the films deposited by non-vacuum methods contain additional states in the vicinity of the band edge due to structural defects within the grains and grain boundaries [35]. This behavior is in consistency with XRD results.

3.2. Effect of gallium composition (x)

After achieving the pure CIGS phase at a T_s of 350 °C, all the deposition parameters were maintained at the same conditions for future investigations. In order to obtain CIGS films with different band gaps, they were grown with various x ranging from 0 to 1, with an interval of 0.25. Fig. 3 shows selected angle XRD pattern of CIGS thin films grown at 350 °C with an increase in Ga content, evaluated by EDAX. The reported content is lower in the precursor solution, and this reduction is more pronounced at higher x values; for instance, solution prepared with x = 1 ended up having 0.82 in

Table 1
Structural parameters of CIGS thin film with gallium content, $x = 0.5$ in the precursor solution deposited at different substrate temperatures (T_s).

T_s (°C)	Peak (112) 2θ (°)	FWHM, β (°)	Crystallite size, D (nm)	Strain, $\varepsilon \times 10^{-4}$ (lines^{-2} m^{-4})	Dislocation density, $\delta \times 10^{15}$ (lines/m^{-2})
350	27.09	0.33	25.72	16.6	1.5
365	27.05	0.35	24.24	17.6	1.7
375	27.03	0.37	22.93	18.6	1.9
385	26.92	0.40	21.21	20.2	2.2
400	26.74	0.42	20.19	21.4	2.4

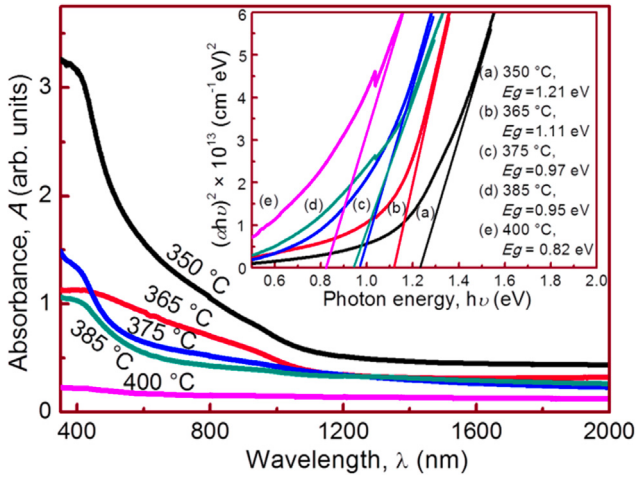

Fig. 2. Optical absorption of CIGS thin film with gallium (x) = 0.5 in the precursor solution deposited at different substrate temperatures (T_s) (the inset figure shows plot of $(\alpha h\nu)^2$ vs. $h\nu$).

the deposited film due to re-evaporation of precursors during deposition. As Ga fraction increases from 0 to 0.82, the diffraction peaks were shifted towards higher angles (26.63°–27.62°) as reported in Fig. 3. The peak marked with "*" in Fig. 3 is due to the $Cu_{2-x}Se$ phase [28]. Fig. 4(a) summarize the FWHM values of (112) XRD

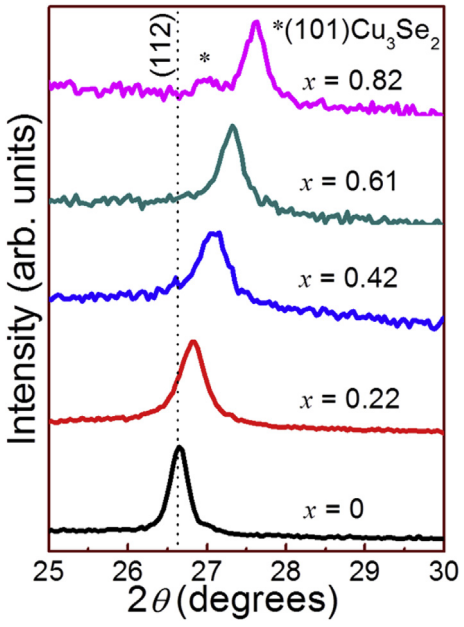

Fig. 3. Selected angle XRD pattern of CIGS thin films deposited at a substrate temperature (T_s) of 350 °C with different Ga/(Ga + In) ratio in precursor solution.

line versus the composition (x). At first glance, FWHM values decreased with increasing x, and this infers an increase in the crystallite size [36]. However, it should be noted that for low gallium concentrations, i.e. $x < 0.22$, only smooth change occurs on FWHM [28].

For all CIGS films, lattice parameters a and c, were calculated manually, using the Cohen method, taking d-spacing into consideration for tetragonal structure, i.e.

$$d = \left(\left(h^2 + k^2\right)/a^2 + l^2/c^2\right)^{-1/2}.$$

Fig. 4(b) shows a graph of the lattice parameters versus Ga/(In + Ga). As Ga content increases, lattice parameters a and c, are observed to decrease for all CIGS films [25,28]. These results suggest small ionic size of Ga (0.62 Å), compared to that of In (0.81 Å) [29]. It is well known that lattice parameters decrease linearly, with increase in Ga fraction. For our CIGS films, the linear decrease is clearly observed. However lattice constant a, exhibiting bowing behavior (Fig. 4(b)) was fitted to second order polynomial equation. The best fitting gives $a\ (x) = 5.78 - 0.089x - 0.215x^2$, with an adjusted r-square value (coefficient of determination) as 0.997. This indicates that the lattice constant a, slightly deviated from Vegard's law. Shirakata et al. [25] noticed similar phenomenon for CIGS films deposited by spray pyrolysis. Fig. 4(b) shows variations in c/a vs. Ga fraction, where c/a value also decreases, with increase in Ga. It is observed that in the range of Ga concentration 0.1–0.2, c/a value is nearly 2 (tetragonal structure), and the distortion of tetragonal structure is more severe at higher Ga concentrations. Similar results were reported by Lee et al. [28], for CIGS films deposited by ultrasonic spray pyrolysis.

Raman measurements have been performed, in order to study the film structure and phase separation, which cannot be obtained by XRD measurements. Fig. 5(a) shows Raman spectra of CIGS films with various x. All Raman spectra exhibit a strong characteristic A1 mode phonon peak (166 cm^{-1} for $CuInSe_2$ and 180 cm^{-1} for $CuIn_{0.18}Ga_{0.82}Se_2$). It is noted that the frequency of A1 mode for CIS film is measured to be 166 cm^{-1}, which is smaller than other reported values [25,37,38]. When the substrate temperature is low during spray of CIS, the as-deposited film shows A1 peak at lower frequency but after thermal annealing, the A1 peak frequency is restored [28]. For films with lower Ga concentrations, no active modes were observed at higher frequency, except for $CuIn_{0.18}Ga_{0.82}Se_2$, where a Raman peak was detected near 266 cm^{-1} emanating from $Cu_{2-x}Se$ which is known to cause degradation of open circuit voltage [37]. Previous Raman studies on CIS films grown by CSP report an intense new peak at 182 cm^{-1}, which is a finger print of sphalerite CIS phase. This peak is located at the slightly higher energy side of A1 mode (174 cm^{-1}), when the growth temperature is low, or the film is In-rich [28,38]. In this study, no extra Raman peak was observed near the A1 mode; and therefore all CIGS films are considered to have chalcopyrite structure. As can be seen in Fig. 5(b), CIGS A1 phonon mode present in the frequency range of 166–180 cm^{-1} is linearly dependent on the composition (x) [28,38]. Thus, Raman spectroscopy can be used, as a

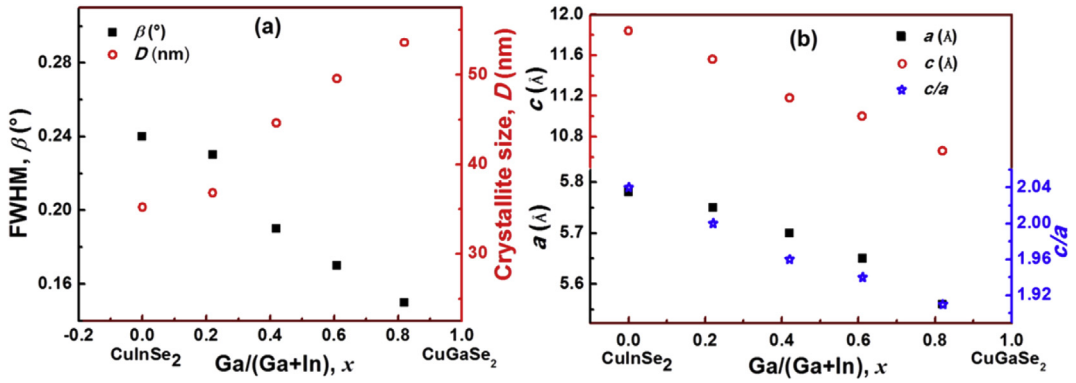

Fig. 4. a) FWHM (β) and crystallite size (D) of (112) peak and b) lattice parameters a and c vs. alloy composition (x) for CIGS thin films with different Ga/(Ga + In) ratio in precursor solution deposited at a substrate temperature (T_s) of 350 °C.

method complementary to EDAX, to calibrate the Ga-fraction in quaternary selenides of unknown stoichiometry.

Compositional dependence of CIS film on Raman spectra is given in Fig. 5(c), with an intense A1 Raman active mode of chalcopyrite phase. In contrast to $Cu_{0.89}InSe_2$ (165 cm^{-1}), the A1 peak position of $Cu_{1.04}InSe_2$ film shifts to higher wave number around 172 cm^{-1}, indicating decrease of the bond-stretching forces with decrease in the Cu content [39]. For $Cu_{0.89}InSe_2$, two weak Raman bands are observed, which are due to the mixed B2(TO)-E(TO) mode at 205 cm^{-1}, and the mixed B2(LO)-E(LO) mode at 220 cm^{-1} [25]. Asymmetric A1 mode with a shoulder at 178 cm^{-1} is noticed for Cu rich film. In fact, similar shoulder peaks have recently been observed in nearly stoichiometric CIS films, grown at substrate temperature of about 400 °C [28], and in Cu-poor or Cu-rich films, grown at temperature of 320 °C by electron beam evaporator [39]. According to the suggestions by Lazewski et al. [40], these shoulder peaks, which are responsible for the broadening of A1 modes, are assigned to E^2 mode of CA-ordered phases. The formation of CA-CIS and Chalcopyrite (CH)–CIS phases proceed through Cu_xSe matrix, at growth temperature of 350–400 °C. Due to atomic diffusion promoted by increasing the deposition time, metastable CA-CIS phases in the films should be fully transformed into stable chalcopyrite-ordered phase, through thermodynamic equilibrium. Following the interdiffusion reaction, there is 1) spontaneous Cu migration from the surface to film interiors and 2) indium anti-diffusion along the intragranular Cu vacancies [41]. This induce a) Cu-poor compounds near the grain boundaries (GBs) on surface, b) Cu-poor materials near the GBs inside the film and c) nearly stoichiometric (Chalcopyrite or CA ordering), at the grain interiors (GIs). Thus, CA ordering phases can be accommodated in some GIs domains. From the Raman spectra in Fig. 5(c), it is reasonable to postulate that the fraction of such CA ordering phase domains should be rather larger in $Cu_{1.04}InSe_2$ films, than that in $Cu_{0.89}InSe_2$. The spontaneous formation of defects, such as Cu vacancies, can enhance the stable (112) preferred orientation which may more likely be correlated with the formation of the CA ordered secondary phases [39].

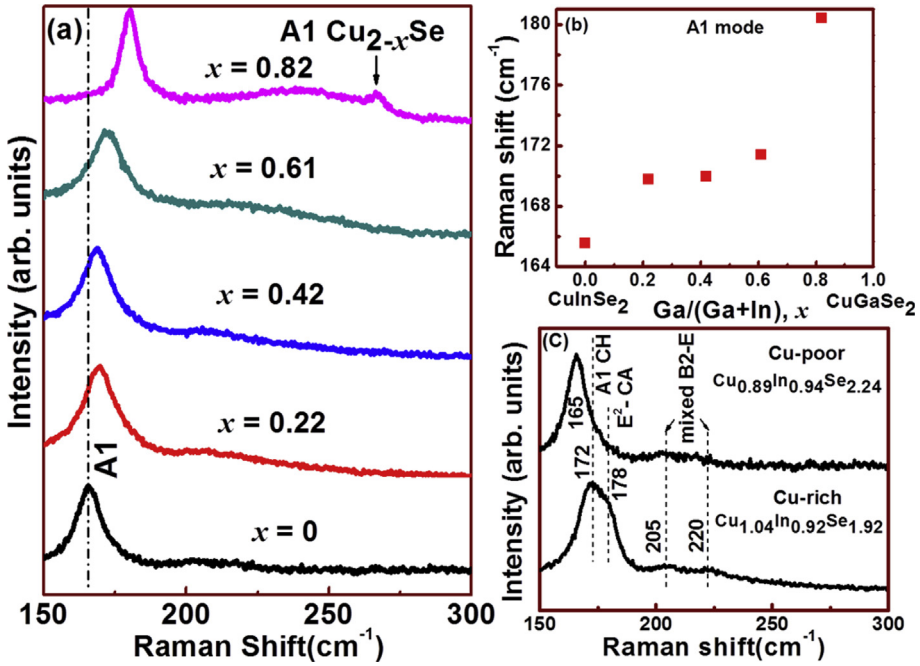

Fig. 5. a) Raman spectra of CIGS thin films deposited at a substrate temperature (T_s) of 350 °C with various Ga/(Ga + In) ratio in precursor solution, b) frequency of A1 phonon mode plotted as a function of alloy composition (x) and c) composition dependence of Raman spectra for CIS films deposited at a T_s of 350 °C.

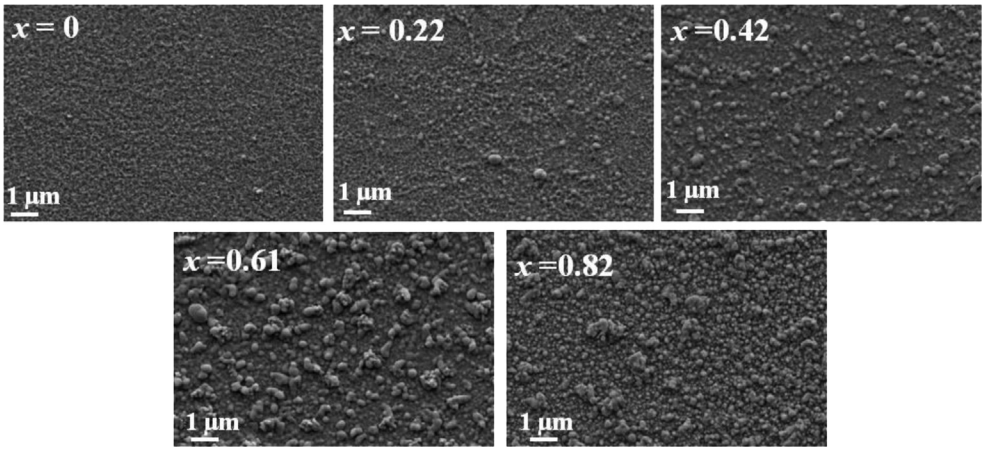

Fig. 6. FESEM images of CIGS thin films deposited at a substrate temperature (T_s) of 350 °C, with different Ga/(Ga + In) ratio in precursor solution.

The micro structural changes induced by gallium incorporation into Cu–In–Se structure are shown in Fig. 6. The films do not show clear grain structure, probably due to lesser thickness (~200 nm), and did show minor influence of Ga incorporation. The chemical composition of these films is given in Table 2 with the composition, x in the film slightly lower than that in the solution. Though the Cu:(In + Ga):Se atomic ratio in the solution is taken as 1:1:3.5, the re-evaporation of gallium and selenium are evident, due to their high vapor pressure [19]. Low gallium content in the films are more pronounced at higher x values, and selenium loss is observed more in quaternary above $x > 0.22$ than in ternary compound. Inter-diffusion of ternaries will be driven by the increase of entropy in quaternary compound, compared to ternary chalcopyrites and therefore, reaction rate depends on the concentration gradient [41]. The Cu atomic ratio in the solution is taken slightly below unity, in order to form Cu-poor films. Cu deficiency increases the majority carrier (hole) concentration (p-type conductivity), by increasing the number of Cu vacancies, which act as electron acceptors [42].

In absorbance spectra, the sharp absorption edge at fundamental absorption region shifts toward lower wavelength, with increasing Ga content from 0, 0.22, 0.42, 0.61 to 0.82 in CIGS films, as shown in Fig. 7(a). A variation of band gap of CIGS with increasing x from 0 to 0.82 is depicted in Fig. 7(b) [43]. Thus, optical studies indicate an increase in the band gap with increasing the gallium content, in agreement with the homogeneous incorporation of gallium into chalcopyrite lattice [44]. A band gap of CIS around 0.9 eV agrees well with the value reported by several authors [45–47]. According to Jaffe et al. [48], the band gap anomaly is influenced by two factors. On one hand, the chemical contribution alters the Se $4p$ − Cu $3d$ hybridization and cation electronegativity. On the other hand, the structural contribution consists in variations in the Se position, and in a small contribution from tetragonal distortions. The structural contribution alters the energy gap of CIS thin films when compositional changes occur, particularly in near-stoichiometric films.

It can also be seen from Fig. 8, that the band gap values systematically increased with an increase in the Ga/(Ga + In) atomic ratio. Although Vegard's law predicts a linear shift for the band gap with increasing x, it was experimentally observed that the band gap versus Ga/(Ga + In) atomic ratio exhibits a bowing behavior, as reported by other authors [44,49], similarly, a least square fit of our experimental data indicated a bowing effect in band gap versus x plot which may be expressed as follows

$$E_g(x) = E_1 + (E_2 - E_1 - b)x + bx^2, \tag{6}$$

where, E_1 and E_2 are the band gap values of CIS and CGS, respectively; while b is the bowing parameter. Second order polynomial curve fitting to the band gap versus Ga/(Ga + In) ratio plot (Fig. 8) shows the following relation to be valid for the specific films shown in Fig. 7. A better measure is obtained by the adjusted r-square value (coefficient of determination) of the fit, and it is determined as 0.993.

$$E_g(x) = 0.90 + 0.58x + 0.14x^2, \tag{7}$$

Concerning the bowing parameter adjusted in our work at 0.14, Wei et al. [50] have observed that 'b' is often dependent on the growth method. Also, the most reproducible values of bowing parameters for CIGS films were within the range of 0.15–0.24 eV [50]. It was noticed that the bowing parameter obtained from the reported [44,46] values of band gap for two stage processed and single crystal CIGS was higher (~0.43). But the value obtained by us (~0.14) is very low, indicating that disorder in the alloy system is quite low. This also suggests that the amount of gallium atoms expected to replace indium has been reduced during the process of alloying, leading to a low band gap of the corresponding films. For instance, if $x = 1$, then from Equation (7), $E_g = 1.62$ eV, which is slightly low, compared with the expected band gap of CGS (~1.68 eV).

Table 2
Compositional data of CIGS thin film with various Ga/(Ga + In) ratios in precursor solution deposited at a substrate temperature (T_s) of 350 °C.

Ga/(Ga + In), x in solution	Cu (at %)	In (at %)	Ga (at %)	Se (at %)	Molecular formula	Ga/(Ga + In)
0 (CIS)	23.23	24.70	–	52.07	$Cu_{0.89}(In_{1.00}Ga_{0.00})_{0.94}Se_2$	0
0.25(CIGS)	21.39	17.69	5.02	55.91	$Cu_{0.76}(In_{0.78}Ga_{0.22})_{0.81}Se_2$	0.22
0.50(CIGS)	23.81	15.53	11.60	49.06	$Cu_{0.97}(In_{0.58}Ga_{0.42})_{1.10}Se_2$	0.42
0.75(CIGS)	22.23	11.60	18.37	47.79	$Cu_{0.93}(In_{0.39}Ga_{0.61})_{1.25}Se_2$	0.61
1(CGS)	21.66	–	22.80	55.55	$Cu_{0.77}(In_{0.00}Ga_{1.00})_{0.82}Se_2$	0.82

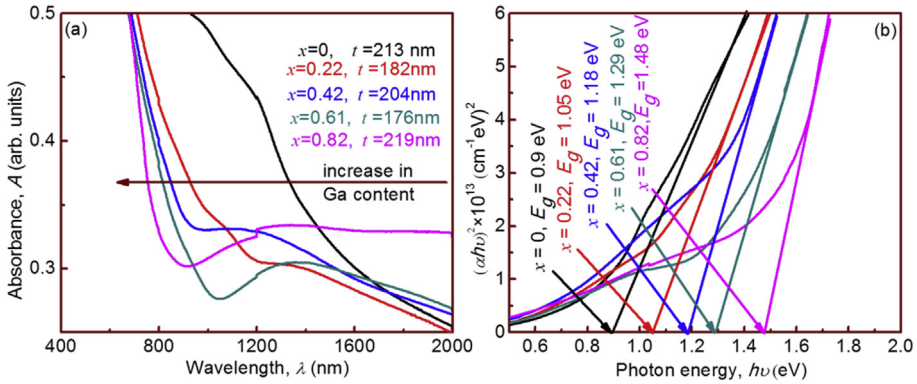

Fig. 7. a) Optical absorption of CIGS thin films deposited at a substrate temperature (T_s) of 350 °C with different Ga/(Ga + In) ratio in precursor solution and b) plot of $(\alpha h\nu)^2$ vs. $h\nu$ for CIGS films deposited at a T_s of 350 °C with varying Ga/(Ga + In) ratio (t is thickness of the film).

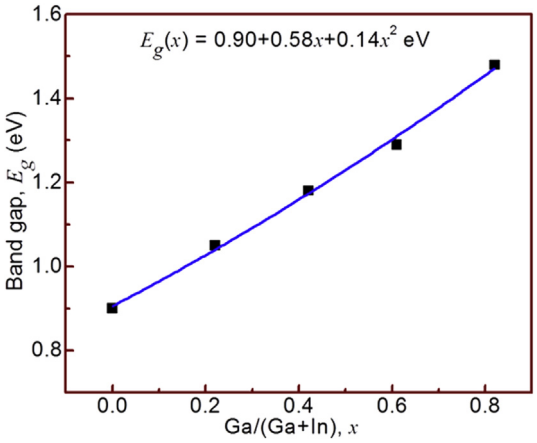

Fig. 8. Variation of band gap (E_g) of CIGS thin films deposited at a substrate temperature (T_s) of 350 °C with different Ga/(Ga + In) ratio in precursor solution as a function of alloy composition (x).

The variations of resistivity, mobility and carrier concentration with x in CIGS thin films are given in Table 3. The resistivity increased from 1.61 to 71.68 Ω-cm, as x increased from 0 (CIS) to 0.42 (CIGS), and then decreased to 4.78 Ω-cm, as the gallium content reached to 0.82. As per reports [43], these parameters decrease with increasing in x. However, several factors, such as sodium doping or chemical composition, also contribute to the electric properties. As we can see from Table 2, with the chemical composition varying from film to film, the obtained values were also randomly distributed. But the majority carrier (hole) concentration is more pronounced, due to Cu deficiency in the films.

3.3. Properties of graded CIGS layer

CIGS films grown with various Ga compositions were stacked together, to form a graded thin film. Preliminary deposition of graded CIGS (x = 1 to 0) layer on glass substrate yielded chalcopyrite phase, as given in Fig. 9, with a preferred (112) orientation. The (112) family of planes corresponds to Cu and In lattice (Se excluded), and it is intuitive that the "annihilation" of In_{Cu} antisites will lead to better ordering of the cations. Such ordering will result in an increase in the periodicity of (112) family of planes, and therefore, a stronger diffraction intensity ("better crystallinity") [51]. Other strong peaks observed from the XRD pattern corresponds to the (220)/(204), (116)/(312) and (316)/(332) orientations. In addition to these lattice planes, one more peak corresponding to (103) plane was also seen, which shows the presence of chalcopyrite structure. An inset figure presented in Fig. 9 indicates a clear tetragonal splitting of (316)/(332) peak which is also a characteristic of chalcopyrite structure. Lattice parameters a = 5.78 Å and c = 11.83 Å showed that the film is tetragonal in nature. The splitting of doublet peak indicates the deviation of tetragonality, c/a = 2.04, induced by Ga substitution [26,28].

The Surface morphology of graded CIGS layer and its cross sectional image are presented in Fig. 10(a) and (b), respectively, which shows a dense and thick (~700 nm) layer. The line scan given in Fig. 10(c) shows a decrease in Ga/(Ga + In) ratio from the bottom layer to the top layer, revealing the graded nature of the film. Cu/(In + Ga) ratio varies from 0.77 to 1.06, from bottom to top. The beneficial effect of such grading on conversion efficiency (19.2%) of CIGS thin film solar cell has been addressed by Ramanathan et al. [52]. A recent study by Lundberg et al. [53] shows that the band gap grading can increase the open circuit voltage (V_{oc}) by 20–30 mV. Another possible cause for unexceptional V_{oc} of devices could be reduced band bending, resulting from a higher than desirable activation energy of the CIGS film. In order to determine the activation energy, a modified Arrhenius plot is used, as shown in Fig. 11. Log (I) is plotted versus the inverse thermal voltage, $1/kT$ as given in the following equation:

$$\mathrm{Log}_{10}I = \log_{10}I_0 - (E_a/kT) \tag{8}$$

In the case of CIGS film on glass, Arrhenius plot of the saturation current I_0 shows a linear dependence with the activation energy E_a.

Table 3
Electrical properties of CIGS thin film with various Ga/(Ga + In) ratios in precursor solution deposited at a substrate temperature (T_s) of 350 °C.

Ga/(Ga + In), x	Resistivity, ρ (Ω-cm)	Mobility, μ (cm^2/V s)	Carrier concentration, p (cm^{-3})
0 (CIS)	1.61	0.17	2.21×10^{19}
0.22(CIGS)	22.86	0.99	2.75×10^{17}
0.42(CIGS)	71.68	1.42	6.09×10^{16}
0.61(CIGS)	19.84	0.84	3.70×10^{17}
0.82(CIGS)	4.78	18.64	6.79×10^{16}

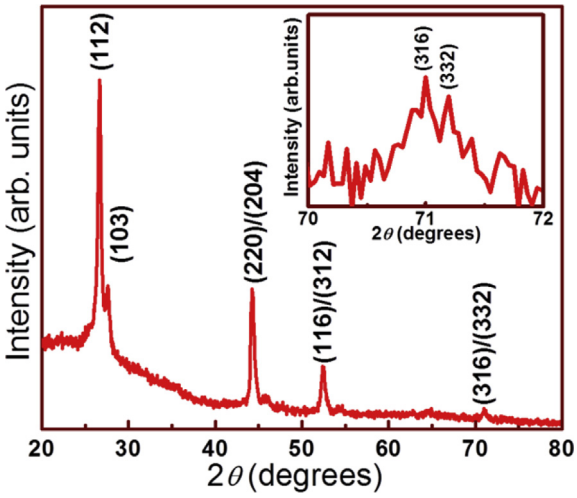

Fig. 9. XRD pattern of graded CIGS ($x = 1$ to 0) layer deposited at a substrate temperature (T_s) of 350 °C (the inset shows selected angle XRD pattern).

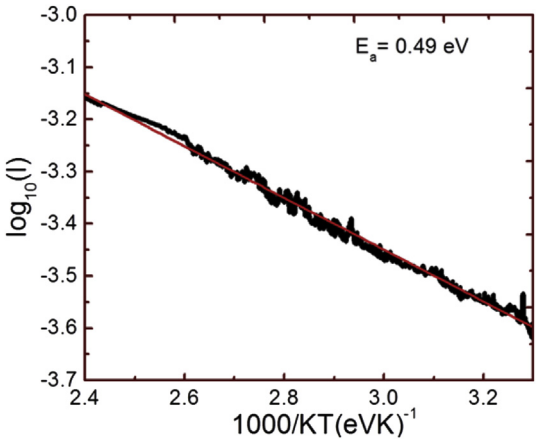

Fig. 11. Modified Arrhenius plot of current vs. temperature with their linear fit curves of graded CIGS ($x = 1$ to 0) layer deposited at a substrate temperature (T_s) of 350 °C.

The activation energy of the CIGS to glass is 0.49 eV (value extracted from graph shown in Fig. 11), while it is 0.5 eV on CIGS/ZnO, as reported by F.J. Haug et al. [54]. It can be concluded that the high temperature step corresponds to the bulk defects (hole traps) in the absorber (activation energy ~0.4–0.5 eV) layer [55]. Thus, damp heat treatment significantly reduces the grain boundaries passivation.

4. Conclusions

The feasibility of preparing graded CIGS layer using simple spray pyrolysis is demonstrated. CIGS thin films were deposited at different substrate temperatures and their structural characterization lead to the optimum temperature as 350 °C yielding single phase films. Raman studies on CIGS films showed a linear dependence of the characteristic A1-mode frequency with increasing

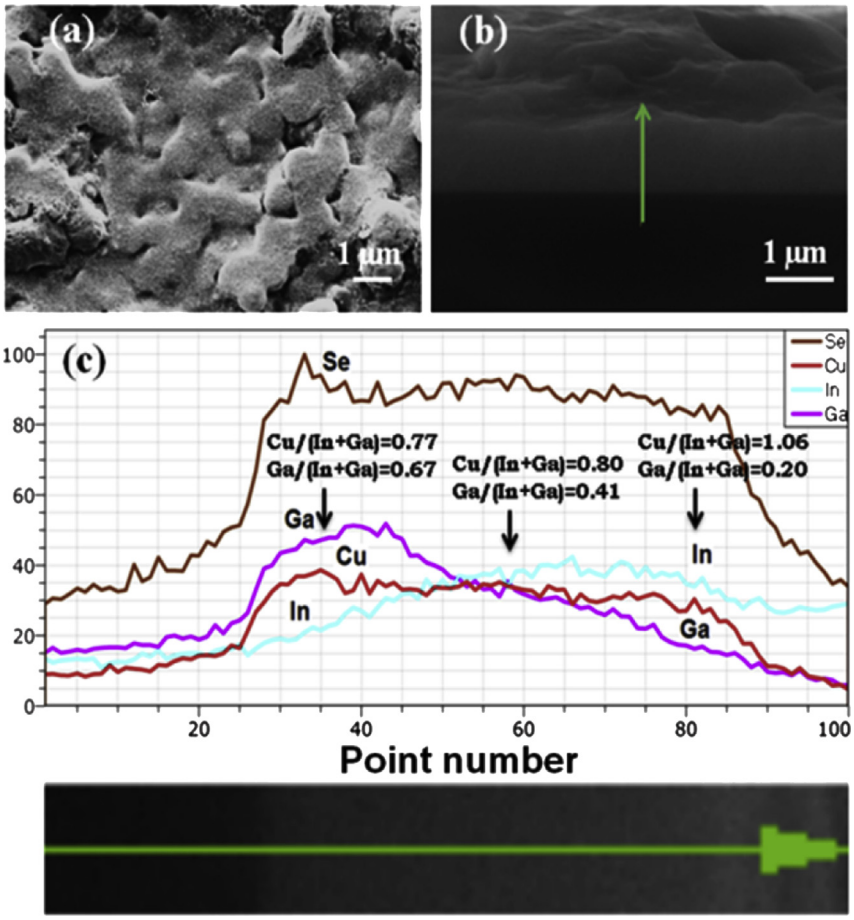

Fig. 10. FESEM analysis of graded CIGS ($x = 1$ to 0) layer deposited at a substrate temperature (T_s) of 350 °C: (a) Surface morphology, (b) cross sectional image and (c) its line scan mapping.

gallium composition. The stoichiometry effect (Cu poor and Cu rich) on A1 Raman mode frequency of CIS films indicated a decrease in the bond-stretching forces with that of Cu content. Gallium incorporation was carried out at optimized substrate temperature, in order to modulate the band gap of CIS thin films. The optical band gap of CIGS films shifted from 0.9 to 1.48 eV, as the gallium content increased from 0 to 0.82, confirming homogeneous incorporation of Ga into the chalcopyrite lattice. Slight bowing behavior of the band gap was observed, with increase of the Ga/(Ga + In) ratio. It is also worth noting that CIGS thin films with gallium grading prepared by spray pyrolysis, in conjunction with post selenization treatment, will be one of the promising ways to fabricate low cost CIGS based solar cells.

Acknowledgments

The authors wish to thank Miguel Galván A (Raman studies) and Adolfo Tavira Fuentes (XRD studies) for their technical assistance. B. J. Babu is thankful to CONACyT for their financial support during his Ph. D. course in Mexico. Also support by the Human Resources Development program (No 20124010203280) of the Korea Institute of Energy Technology Evaluation and Planning (KETEP) grant funded by the Korea Government Ministry of Trade, Industry and Energy is acknowledged. One of the authors wishes to acknowledge the support from BrainPool project (11-150-152-1600-1658) from MSIP, Korea. Authors wish to thank ICyTDF for the financial support through the project 326/11.

References

[1] K.L. Chopra, P.D. Paulson, V. Dutta, Thin-film solar cells: an overview, Prog. Photovolt. Res. Appl. 12 (2004) 69–92.
[2] V.F. Gremenok, E.P. Zaretskaya, V.B. Zalesski, K. Bente, W. Schmitz, R.W. Martin, H. Moller, Preparation of Cu(In,Ga)Se_2 thin film solar cells by two-stage selenization processes using N_2 gas, Sol. Energy Mater. Sol. Cells 89 (2005) 129–137.
[3] S. Shirakata, T. Terasako, T. Kariya, Properties of $CuIn(S_xSe_{1-x})_2$ polycrystalline thin films prepared by chemical spray pyrolysis, J. Phys. Chem. Solids 66 (2005) 1970–1973.
[4] E. Halgand, J.C. Bernede, S. Marsillac, J. Kessler, Physico- chemical characterisation of Cu(In, Al)Se_2 thin film for solar cells obtained by a selenisation process, Thin Solid Films 480/481 (2005) 443–446.
[5] P. Jackson, D. Hariskos, E. Lotter, S. Paetel, R. Wuerz, R. Menner, W. Wischmann, M. Powalla, New world record efficiency for Cu(In, Ga)Se_2 thin-film solar cells beyond 20%, Prog. Photovolt. Res. Appl. 19 (2011) 894–897.
[6] Press release dated 22nd September 2014, accessed on 24th November 2014, (http://www.pv-magazine.com/news/details/beitrag/zsw-sets-217-thin-film-efficiency-record_100016505/#axzz3IAXN9AUl).
[7] A. Chirila, S. Buecheler, F. Pianezzi, P. Bloesch, C. Gretener, A.R. Uhl, C. Fella, L. Kranz, J. Perrenoud, S. Seyrling, R. Verma, S. Nishiwaki, Y.E. Romanyuk, G. Bilger, A.N. Tiwari, Highly efficient Cu(In,Ga)Se_2 solar cells grown on flexible polymer films, Nat. Mater. 10 (2011) 857–861.
[8] A. Chirila, P. Reinhard, F. Pianezzi, P. Bloesch, A.R. Uhl, C. Fella, L. Kranz, D. Keller, C. Gretener, H. Hagendorfer, D. Jaeger, R. Erni, S. Nishiwaki, S. Buecheler, A.N. Tiwari, Potassium-induced surface modification of Cu(In,Ga)Se_2 thin films for high-efficiency solar cells, Nat. Mater. 12 (2013) 1107–1111.
[9] P. Bommersbach, L. Arzel, M. Tomassini, E. Gautron, C. Leyder, M. Urien, D. Dupuy, N. Barreau, Influence of Mo back contact porosity on co-evaporated Cu(In,Ga)Se_2 thin film properties and related solar cell, Prog. Photovolt. Res. Appl. 21 (2011) 332–343.
[10] I. Repins, M.A. Contreras, B. Egaas, C. DeHart, J. Scharf, C.L. Perkins, B. To, R. Noufi, 19.9%-efficient ZnO/CdS/$CuInGaSe_2$ solar cell with 81.2% fill factor, Prog. Photovolt. Res. Appl. 16 (2008) 235–239.
[11] M. Kaelin, D. Rudmann, A.N. Tiwari, Low cost processing of CIGS thin film solar cells, Sol. Energy 77 (2004) 749–756.
[12] C.J. Hibber, E. Chassaing, W. Liu, D.B. Mitzi, D. Lincot, A.N. Tiwari, Non-vacuum methods for formation of Cu(In,Ga)$(Se,S)_2$ thin film photovoltaic absorbers, Prog. Photovolt. Res. Appl. 18 (2010) 434–452.
[13] T.K. Todorov, O. Gunawan, T. Gokmen, D.B. Mitzi, Solution-processed Cu(In,-Ga)$(S,Se)_2$ absorber yielding a15.2% efficient solar cell, Prog. Photovolt. Res. Appl. 21 (2013) 82–87.
[14] B.M. Basol, M. Pinarbasi, S. Aksu, J. Wang, Y. Matus, T. Johnson, Y. Han, M. Narasimham, B. Metin, Electroplating based technolgy for roll-to-roll manufacturing, in: 23rd European Photovoltaic Solar Energy Conference, 2008. Valencia.
[15] J. vanDuren, D. Jackrel, F. Jacob, C. Leidholm, A. Pudov, M. Robinson, Y. Roussillon, The next generation in thin film photovoltaic process technology, in: Conference Record of the Seventeenth International Photovoltaic Science and Engineering Conference, 2007. Fukuoka, Japan.
[16] Q. Guo, G.M. Ford, R. Agrawal, H.W. Hillhouse, Ink formulation and low-temperature incorporation of sodium to yield 12% efficient Cu(In,Ga)(S,Se)2 solar cells from sulfide nanocrystal inks, Prog. Photovolt. Res. Appl. 21 (2013) 64–71.
[17] S. Duchemin, J. Bougnot, A. El Ghzizal, K. Belghit, Studies on the improvement of sprayed CdS-$CuInSe_2$ solar cells, in: Proceedings of the 9th European Photovoltaic Solar Energy Conference, 1989, pp. 476–479.
[18] B. Pamplin, R.S. Feigelson, Spray pyrolysis of $CuInSe_2$ and related ternary semiconducting compounds, Thin Solid Films 60 (1979) 141–146.
[19] A.N. Tiwari, D.K. Pandya, K.L. Chopra, Electrical and optical properties of single-phase $CuInS_2$ films prepared using spray pyrolysis, Thin Solid Films 130 (1985) 217–230.
[20] C.R. Abernathy, C.W. Bates Jr., A.A. Anani, B. Haba, G. Smestad, Production of single phase chalcopyrite $CuInSe_2$ by spray pyrolysis, Appl. Phys. Lett. 45 (1984) 890–892.
[21] J. Bougnot, S. Duchemin, M. Savelli, Chemical spray pyrolysis of $CuInSe_2$ thin films, Sol. Cells 16 (1986) 221–236.
[22] M.S. Tomar, F.J. Garcia, A ZnO/P-$CuInSe_2$ thin film solar cell prepared entirely by spray pyrolysis, Thin Solid Films 90 (1982) 419–423.
[23] T. Terasako, S. Inoue, T. Kariya, S. Shirakata, Three- stage growth of Cu-In-Se polycrystalline thin films by chemical sparay pyrolysis, Sol. Energy Mater. Sol. Cells 91 (2007) 1152–1159.
[24] B.J. Brown, C.W. Bates Jr., Preparation and characterization similarities in the chemical mechanisms of $CuInSe_2$ and CdS thin film formation by chemical spray pyrolysis, Thin Solid Films 188 (1990) 301–305.
[25] S. Shirakata, Y. Kannaka, H. Hasegawa, T. Kariya, S. Isomura, Properties of Cu(In,Ga)Se_2 thin films prepared by chemical spray pyrolysis, Jpn. J. Appl. Phys. 38 (1999) 4997–5002.
[26] K.T. Ramakrishna Reddy, R.B.V. Chalapathy, Structural properties of $CuGa_xIn_{1-x}Se_2$ thin films deposited by spray pyrolysis, Cryst. Res. Technol. 34 (1999) 127–132.
[27] K.T. Ramakrishna Reddy, R.B.V. Chalapathy, Spray pyrolysis of $CuGa_xIn_{1-x}Se_2$ thin films-electrical and optical properties, in: Salford, U.K., September 8–12, 1997, Inst. Phys. Conf, 152, 1997, p. 317.
[28] D.Y. Lee, S. Park, J. Kim, Structural analysis of CIGS film prepared by chemical spray deposition, Curr. Appl. Phys. 11 (2011) S88–S92.
[29] B. Vidhya, S. Velumani, J.A. Arenas-Alatorre, Arturo Morales-Acevedo, R. Asomoza, J.A. Chavez-Carvayar, Structural studies of mechano-chemically synthesized $CuIn_{1-x}Ga_xSe_2$ nanoparticles, Mater. Sci. Eng. B 174 (2010) 216–221.
[30] B. Vidhya, S. Velumani, R. Asomoza, Effect of milling time and heat treatment on the composition of $CuIn_{0.75}Ga_{0.25}Se_2$ nanoparticle precursors and films, J. Nanopart. Res. 13 (2011) 3033–3042.
[31] S. Velumani, B.J. Babu, B. Vidhya, P. Reyes, A. Angeles, R. Asomoza, Preparation, deposition of Cu$(In_{1-x}Ga_x)Se_2$ nanopowder thin films by non-vacuum processes and its characterization, in: Seattle, U.S.A., June 19–24, 2011, 37th IEEE Photovoltaic Specialist Conference, 1, 2011, p. 440.
[32] B.J. Babu, S. Velumani, Arturo Morales-Acevedo, R. Asomoza, Properties of CuInGaSe thin films prepared by chemical spray pyrolysis, in: Tuxtla Gutierrez, Mexico, September 8–10, 2010, 7th International Conference on Electrical Engineering Computing Science and Automatic Control, 2010, ISBN 978-1-4244-7312-0, p. 582.
[33] B.J. Babu, S. Velumani, R. Asomoza, An (ITO OR AZO)/ZnO/Cu$(In_{1-x}Ga_x)Se_2$ superstrate thin film solar cell structure prepared by spray pyrolysis, in: Seattle, U.S.A., June 19–24, 2011, 37th IEEE Photovoltaic Specialist Conference, 1, 2011, p. 1238.
[34] C.W. Bates Jr., K.F. Nelson, S. Atiq Raza, J.B. Mooney, J.M. Recktenwald, L. Macintosh, R. Lamoreaux, Spray pyrolysis and heat treatment of $CuInSe_2$ for photovoltaic applications, Thin Solid Films 88 (1982) 279–283.
[35] E. Ahmed, R.D. Tomlinson, R.D. Pilkington, A.E. Hill, W. Ahmed, Nasar Ali, I.U. Hassan, Significance of substrate temperature on the properties of ash evaporated $CuIn_{0.75}$ $Ga_{0.25}Se_2$ thin films, Thin Solid Films 335 (1998) 54–58.
[36] F.B. Dejene, The structural and material properties of $CuInSe_2$ and Cu(In,Ga) Se_2 prepared by selenization of stacks of metal and compound precursors by Se vapor for solar cell applications, Proc. SPIE 7045 (2008) 70450H.
[37] H. Miyazakia, R. Mikamia, A. Yamadab, M. Konagaia, Cu(InGa)Se_2 thin film absorber with high Ga contents and its application to the solar cells, J. Phys. Chem. Solids 64 (2003) 2055–2058.
[38] D. Papadimitriou, N. Esser, C. Xue, Structural properties of chalcopyrite thin films studied by Raman spectroscopy, Phys. Status Solidi B 242 (13) (2005) 2633–2643.
[39] C.M. Xu, X.L. Xu, J. Xu, X.J. Yang, J. Zuo, N. Kong, W.H. Huang, H.T. Liu, Composition dependence of the Raman A1 mode and additional mode in tetragonal Cu–In–Se thin films, Semicond. Sci. Technol. 19 (2004) 1201–1206.
[40] J. Lazewski, H. Neumann, K. Parlinski, G. Lippold, B.J. Stanbery, Lattice dynamics of CuAu-ordered $CuInSe_2$, Phys. Rev. B 68 (2003) 144108-1–144108-5.
[41] F. Hergert, S. Jost, R. Hock, M. Purwins, A crystallographic description of experimentally identified formation reactions of Cu(In,Ga)Se_2, J. Solid State Chem. 179 (2006) 2394–2415.

[42] K. Marianna, R. Mikko, L. Markku, Thin film deposition methods for $CuInSe_2$ solar cells, Crit. Rev. Solid State Mater. Sci. 30 (1) (2005) 1–5.
[43] Subba Ramaiah Kodigala, Thin Films and Nanostructures: $Cu(In_{1-x}Ga_x)Se_2$ Based Thin Film Solar Cells, Academic Press, MA, 2010.
[44] F.B. Dejene, V. Alberts, Structural and optical properties of homogeneous $Cu(In,Ga)Se_2$ thin films prepared by thermal reaction of InSe/Cu/GaSe alloys with elemental Se vapour, J. Phys. D. Appl. Phys. 38 (2005) 22–25.
[45] Y.D. Tembhurkar, J.P. Hirde, Structural, optical and electrical properties of spray pyrolytically deposited films of copper indium diselenide, Thin Solid Films 215 (1992) 65–70.
[46] M.C. Joliet, C. Antoniadis, L.D. Laude, Laser induced synthesis of thin $CuInSe_2$ films, Thin Solid Films 126 (1985) 143–148.
[47] G.K. Padam, Composition and structure of chemically deposited $CuInSe_2$ thin films, Mat. Res. Bull. 22 (1987) 789–794.
[48] J.E. Jaffe, A. Zunger, Theory of the band-gap anomaly in ABC_2 chalcopyrite semiconductors, Phys. Rev. B 29 (1984) 1882–1906.
[49] S. Roy, P. Guha, S.N. Kundu, H. Hanzawa, S. Chaudhuri, A.K. Pal, Characterization of $Cu(In, Ga)Se_2$ films by Raman scattering, Mater. Chem. Phys. 73 (2002) 24–30.
[50] S.H. Wei, A. Zunger, Band offsets and optical bowings of chalcopyrites and Zn-based II-VI alloys, J. Appl. Phys. 78 (1995) 3846–3856.
[51] M.A. Contreras, B. Egaas, P. Dippo, J. Webb, J. Granata, K. Ramanathan, S. Asher, A. Swartzlander, R. Noufi, On the role of Na and modifications to CIGS absorber materials using thin MF (M=Na, K, Cs) precursor layers, in: Conference Record of the Twenty Sixth IEEE Photovoltaic Specialists Conference, 1997, pp. 359–362.
[52] K. Ramanathan, M.A. Contreras, C.L. Perkins, S. Asher, F.S. Hasoon, J. Keane, D. Young, M. Romero, W. Metzger, R. Noufi, J. Ward, A. Duda, Properties of 19.2% efficiency $ZnO/CdS/CuInGaSe_2$ thin-film solar cells, Prog. Photovolt. Res. Appl. 11 (2003) 225–230.
[53] O. Lundberg, M. Bodegard, J. Malmstrom, L. Stolt, Influence of the $Cu(In,Ga)Se_2$ thickness and Ga grading on solar cell performance, Prog. Photovolt. Res. Appl. 11 (2003) 77–88.
[54] F.J. Haug, D. Rudmann, A. Romeo, H. Zogg, A.N. Tiwari, Electrical properties of the heterojunction in $Cu(In,Ga)Se_2$ superstrate solar cells, in: 3rd World Conference on Photovoltaic Solar Energy Conversion, Osaka, 2003.
[55] A. Kubiaczyk, M. Nawrocka, M. Igalson, Admittance measurements on CIGS solar cells, Opto-Electron. Rev. 8 (2000) 378–381.